Mapping Surface Oil Extent From the Deepwater Horizon Oil Spill Using ASCAT Backscatter

Richard D. Lindsley, *Student Member, IEEE*, and David G. Long, *Fellow, IEEE*

***Abstract*—The 2010 Deepwater Horizon oil spill in the Gulf of Mexico covered a sufficiently large area to be observed by the European Space Agency Advanced Scatterometer (ASCAT) on MetOp-A. In this paper, ASCAT data and numerically computed winds from the European Centre for Medium-Range Weather Forecasts (ECMWF) are used to map the spatial extent of oil on the ocean surface over the duration of the spill event. Surface oil alters the ocean radar scattering properties, resulting in a difference between the measured backscatter and the backscatter that would be measured if oil were not present. Wind scatterometers infer the near-surface wind speed and direction using the wind geophysical model function (GMF) in conjunction with measured radar backscatter. The oil-altered backscatter error propagates through the wind retrieval process to create a difference in ASCAT-inferred winds and actual winds. Numerically computed vector winds from ECMWF are compared against ASCAT-inferred vector winds. The GMF is applied to ECMWF winds to create a predicted backscatter value to compare against ASCAT-measured backscatter. Large differences in wind or backscatter indicate areas of the ocean surface affected by oil. An objective function is developed to choose an appropriate threshold level to flag the oil-contaminated regions. Data from other sensors corroborate the ASCAT oil extent mapping.**

***Index Terms*—Oil pollution, radar remote sensing, scatterometer, spaceborne radar.**

I. Introduction

THE OIL spill from the *Deepwater Horizon* oil rig in the Gulf of Mexico is one of the largest environmental disasters in recent history. The consequences from the roughly 4.4 Mbbl that leaked [1] will continue long after the July 15, 2010, capping of the well. A time-series estimate of the extent and shape of the oil on the ocean surface is beneficial for estimating the amount of oil as a function of time and its impact on ocean life and human industries.

Active microwave sensors are often used for remote detection of oil spills by virtue of their all-weather performance in both day and night conditions. Historically, synthetic aperture radar (SAR) instruments have been used since the spatial resolution—on the order of a hundred meters or less for a spaceborne SAR—is fine enough to resolve many oil spills [2]–[5]. Wind scatterometers are a related class of active microwave instruments with a resolution that is more coarse—on the order of a few kilometers [6], [7]. Nevertheless, the processes that enable oil detection using SAR images are the same for scatterometer data.

The spatial extent of the 2010 Deepwater Horizon oil slick is large enough to be resolvable by the European Space Agency Advanced Scatterometer (ASCAT) on MetOp-A, particularly when processed with resolution-enhancement algorithms. By exploiting the effects of surface oil on the radar backscatter from ocean waves, the surface extent may be mapped (resolution ≈5 km) by examining processed data from ASCAT.

ASCAT is a spaceborne wind scatterometer operating in polar orbit [6]. Like other wind scatterometers, ASCAT indirectly measures near-surface neutral-stability vector ocean winds at a height of 10 m (U_{10}) by measuring backscattered microwave power over the ocean at various incidence and azimuth angles. An empirically derived geophysical model function (GMF) that relates backscatter with U_{10} vector (speed and direction) winds is used to infer the vector wind from backscatter measurements taken at multiple azimuth angles.

This paper presents a method for surface oil extent mapping by determining the difference between predicted and ASCAT-observed quantities. Both wind and backscatter differences are used. Predicted wind or predicted backscatter is found from numerical-weather-predicted (NWP) winds provided by the European Centre for Medium-Range Weather Forecasts (ECMWF). Measured winds or measured backscatter is provided by ASCAT. A suitable threshold is chosen to classify ocean regions as oil affected or oil free. The mapped surface oil extent is validated using data from other sensors. Lacking information on oil thickness or volume, we make no attempt to estimate thickness or volume.

Background information on ASCAT, the GMF, and the effects of surface oil is presented in Section II. The methodology for surface oil extent mapping is described in Section III. Results are shown for selected case studies, and the performance of the methods is evaluated in Section IV.

II. Background

The Deepwater Horizon oil spill is located around 29° latitude. For ASCAT, a maximum of two passes per day is possible (ascending and descending) at this location, but in practice, only about eight passes per ten-day period adequately cover the spill region.

Launched in 2006 aboard MetOp-A, ASCAT is in a sun-synchronous polar orbit. It is a real-aperture scatterometer operating in the C-band (5.255 GHz) with three fan beams on either side of the MetOp ground track. This forms approximately a

Manuscript received June 9, 2011; revised August 10, 2011; accepted October 8, 2011. Date of publication December 13, 2011; date of current version June 20, 2012.

The authors are with the Microwave Earth Remote Sensing Laboratory, Brigham Young University, Provo, UT 84602 USA (e-mail: rlindsley@byu.net; long@ee.byu.edu).

Color versions of one or more of the figures in this paper are available online at http://ieeexplore.ieee.org.

Digital Object Identifier 10.1109/TGRS.2011.2174369

1820-km-wide ground swath with a 720-km-wide gap at nadir. ASCAT operates in vertical-polarization mode only. The three fan beam antennas are positioned such that their measurements are at different azimuth angles, helping resolve ambiguities in the GMF inversion process [6].

The radar backscatter, i.e., normalized radar cross section σ°, of the ocean surface is measured by each of the antennas. The CMOD5.n GMF describes σ° as a function of U_{10} and other parameters, including the incidence angle and the azimuth angle relative to wind direction [8]. Because the GMF is not a one-to-one function, inversion of the GMF (i.e., solving for U_{10} in terms of σ°) leads to nonunique solutions or ambiguities. These wind ambiguities are reduced by using σ° measurements of each sample point in the swath at different azimuth angles. Spatial consistency constraints are used to select a unique vector wind [9], [10].

For each location in the ASCAT swath, three σ° measurements are collected, one each for the antenna "looks": fore, mid, and aft. The middle look is at a slightly lower range of incidence angles than the fore and aft looks [6]. High-resolution σ° imagery is generated for each look using the AVE algorithm. The AVE algorithm is a weighted average of each σ° measurement on a high-resolution grid using estimates of the ground footprint of each measurement [11]–[15]. ASCAT σ° is computed on a 4.45 km by 4.45 km grid using AVE. These high-resolution σ° images are the basis of ultrahigh-resolution (UHR) ASCAT wind, a wind product containing UHR U_{10} vector wind.

At the oblique incidence angle range used for scatterometers (30°–60° for ASCAT), the scattering mechanism from the ocean surface roughness is due to Bragg scattering. When ocean wave wavelengths of λ_o fulfill the Bragg resonance condition

$$\lambda_o = n\lambda_r/2\sin\theta_i, \qquad n = 1, 2, \ldots \tag{1}$$

where λ_r is the radar wavelength and θ_i is the incidence angle, the electromagnetic waves constructively self-interfere to enhance the surface σ° value [16]. For the radar frequency and range of incidence angles used by ASCAT, capillary–gravity ocean waves with a wavelength of 3.5–6.7 cm are responsible for Bragg scattering $(n = 1)$.

While modulated by larger gravity waves, Bragg waves are generally in equilibrium with near-surface wind speed [7]. Higher winds generate more Bragg waves, leading to greater σ° values for greater wind speeds. Because oil is more viscous than seawater, oil on the ocean surface dampens the amplitude of Bragg waves. This modifies the σ° of the affected area because the smoother ocean surface reflects less microwave power back to the scatterometer. The σ° measurement of the oil-contaminated area is thus lower than the oil-free case [2], [4], [17], [18].

The presence of oil in σ° imagery is determined by the contrast difference between oil-affected σ° and non-oil-affected σ°. The value of σ° over the ocean depends on many factors—geophysical, such as near-surface wind speed and direction; instrument specific, such as the frequency, polarization, and incidence and azimuth angles; and the type and the volume or thickness of surface oil.

While the crude oil from the Deepwater Horizon oil spill dominates Bragg wave dampening observed by ASCAT, other sources—both oil and otherwise—can result in patches of dampened backscatter. These include biogenic oil slicks produced by plankton and fish, natural oil seeps from the ocean floor, organic wastes from fish processing ships, and changes in the water–ocean interface, such as that from upwelling [17]. Although covering a much smaller area than the Deepwater Horizon spill, these sources can lead to false positives in oil spill detection, referred to as "look-alikes." Techniques to reduce look-alikes include using multifrequency and multipolarization instruments [3]–[5], [19]; applying *a priori* knowledge of geographic information, historical human and animal activity, and shipping lanes; and using different remote sensors that detect oil under mechanisms other than Bragg scattering (such as microwave radiometers or infrared, optical, or ultraviolet sensors) [2], [17]. Many of these look-alikes are too small to be resolvable by ASCAT. However, low-wind-speed regions that are large enough to be detected by ASCAT can have very low backscatter and potentially be confused with oil-covered ocean surface.

Another geophysical influence on backscatter is precipitation. At C-band, rain generally increases the observed σ° [20]. As with oil-contaminated σ° measurements, this backscatter bias results in a wind speed bias after wind retrieval. However, measured σ° and retrieved wind speeds are dampened by oil, whereas they are increased by rain. As detailed hereinafter, our method for oil detection evaluates backscatter or wind speed less than their predicted values. Values of backscatter or wind speed greater than those predicted are discarded. This effectively excludes measurements affected by rain.

A challenge to oil detection using σ° is that the σ° dampening depends on wind speed. If winds are below a threshold wind speed, the ocean surface is not sufficiently roughened to provide a contrast between the oil-contaminated surface and the oil-free surface. For C-band scatterometers such as ASCAT, this threshold is $\sim$3–4 m/s [21]. Additionally, if the winds are too high (>7–10 m/s), the surface oil mixes down into the water and may be less detectable. The wind speed range that is best suited for oil detection is therefore about 3–10 m/s. Previous papers have recognized the importance of factoring wind speed in surface oil detection [2], [18] and have done so, for example, as part of synergistic data methods [22]. Rather than relying solely upon σ° measurements to detect oil, the method presented in this paper incorporates the effects of wind as part of the detection process. Wind fields from numerical weather prediction products are used, such as from ECMWF.

III. Method

Surface oil is detectable given sufficient differences between the observed and predicted winds or backscatter. The wind error is found by comparing the ASCAT-retrieved winds with ECMWF winds. Similarly, the backscatter error is determined by comparing ASCAT σ° measurements with predicted σ° values derived from ECMWF winds. When the error is greater than some threshold, the region is flagged as having surface

oil. The threshold is determined by minimizing an objective function.

A. Wind Error

For comparison of wind data, ECMWF U_{10} is used. In this section, the notation U_{10} refers to ECMWF-derived winds, and $\hat{U}_{10}$ represents winds found from ASCAT σ° after wind retrieval using the GMF. ECMWF winds have a temporal resolution of 6 h and a spatial resolution of $1^\circ \times 1^\circ$. The two ECMWF wind fields nearest in time to an ASCAT pass are bilinearly interpolated in space to match the ASCAT measurement locations. The two interpolated wind fields are then interpolated in time to the ASCAT pass. This forms a trilinear interpolation to find the interpolated U_{10} corresponding to each $\hat{U}_{10}$.

Although the interpolated U_{10} has the same resolution of $\hat{U}_{10}$, it has limited high-frequency spatial content. A direct comparison of U_{10} with $\hat{U}_{10}$ therefore removes the low spatial frequency winds but preserves any small-scale structure. The wind speed error $\epsilon_{|U_{10}|}$ is defined as

$$\epsilon_{|U_{10}|} = |U_{10}| - |\hat{U}_{10}| \tag{2}$$

and the wind direction error $\epsilon_{\angle U_{10}}$ is defined as

$$\epsilon_{\angle U_{10}} = \angle U_{10} - \angle \hat{U}_{10}. \tag{3}$$

Due to instrument noise and biases in ECMWF winds versus ASCAT winds, $\epsilon_{|U_{10}|}$ and $\epsilon_{\angle U_{10}}$ are rarely zero. However, the wind speed error $\epsilon_{|U_{10}|}$ is anticipated to be positive in regions affected by surface oil since the dampened σ° from the oil is manifested after GMF inversion as lower wind speed. Thus, large positive values of $\epsilon_{|U_{10}|}$ are used as a metric to map the oil surface extent. The effect of oil on wind direction is unclear, but large $\epsilon_{\angle U_{10}}$ could indicate the presence of oil.

B. Backscatter Error

To compute the reference backscatter, ECMWF winds are trilinearly interpolated to match the measurement geometry of ASCAT. The interpolated winds are input to the CMOD5.n GMF using the observation geometry to find the predicted backscatter for each of the three looks. The difference between the predicted backscatter σ° (from ECMWF winds) and the measured backscatter $\hat{\sigma}^\circ$, (from ASCAT) for each look k is

$$\sigma_k^\circ - \hat{\sigma}_k^\circ = \epsilon_k \tag{4}$$

where ϵ_k is the error for look k. As with wind error, some error is anticipated from noise, although the predicted value of ϵ_k is positive in the presence of oil.

We combine the three error terms by stacking them into a vector $\bar{\epsilon} = [\epsilon_{\text{fore}} \epsilon_{\text{mid}} \epsilon_{\text{aft}}]^T$. The ℓ_2 norm of $\bar{\epsilon}$, defined as

$$\|\bar{\epsilon}\|_2 = \sqrt{\epsilon_{\text{fore}}^2 + \epsilon_{\text{mid}}^2 + \epsilon_{\text{aft}}^2} \tag{5}$$

is used as a metric to map the surface oil extent by combining data from all available looks. $\|\bar{\epsilon}\|_2$ is defined as the backscatter error. While the fore and aft measurements are at similar incidence angles, the midbeam σ° is at a lower incidence angle range and is, therefore, generally brighter. Weighting the squared error contributions separately could be used to account for this difference. However, in this paper, we use equal weights for all three looks.

C. Oil Extent Validation

Oil coverage products from the Experimental Marine Pollution Surveillance Report (EMPSR) are used to validate the results. The EMPSR is an experimental product produced by the National Oceanic and Atmospheric Administration. Analysts interpret SAR and visible imagery from satellites to estimate the surface oil extent of the spill [23]. EMPSR does not report the oil thickness or volume.

The EMPSR product used is the daily composite shapefile, a vector-based geospatial representation of surface oil extent based on the available satellite imagery for the day. EMPSR products are not available every day, so only ASCAT passes that coincide with EMPSR data are used.

D. Threshold Determination

The backscatter and wind errors are thresholded to determine oil-affected and oil-free regions. To find a threshold value for each pass, the value that minimizes a simple objective function is determined. We choose a function to express the relationship between probability of false alarm and probability of detection. The objective function is defined as the weighted combination of two values: the number of oil-flagged pixels that fall within the EMPSR region limits and the number of oil pixels that are outside the EMPSR region. This is expressed as

$$f(\nu) = 1/g + \alpha b \tag{6}$$

where ν is the threshold value, $f(\cdot)$ is the objective function, g is the number of correctly classified pixels, b is the number of incorrectly classified pixels, and α is a weighting parameter. The weighting factor α is set to an appropriate metric weighting, so as to achieve some desired probability of false alarm rate. For this paper, we subjectively choose $\alpha = 1 \times 10^{-5}$.

For both backscatter and wind speed errors, the threshold level ν for each pass is found which minimizes (6), the objective function. Fig. 1 shows values of g, b, and f for different threshold levels ν for a typical ASCAT pass. The minimum of $f(\nu)$ is indicated in the figure.

IV. Results

For the duration of the oil leak (April 21–August 25), 204 ASCAT passes over the spill region are available. Of these, 118 have corresponding EMPSR data, and 11 are selected as case studies. For each ASCAT pass over the oil spill region, interpolated ECMWF winds are compared with ASCAT-derived winds to find wind errors $\epsilon_{|U_{10}|}$ and $\epsilon_{\angle U_{10}}$. The measured σ° for each look is compared with the predicted σ° obtained from interpolated ECMWF winds and the CMOD5.n GMF

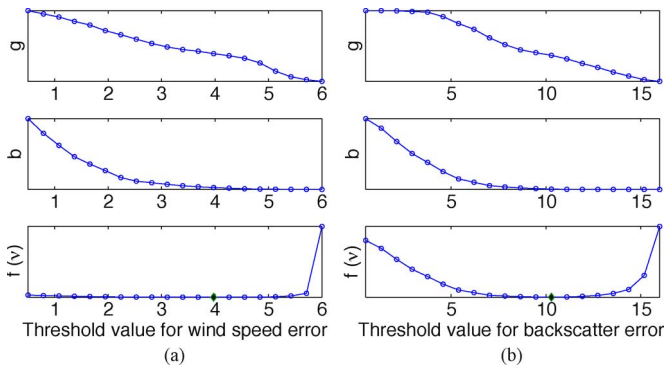

Fig. 1. Threshold objective function and its components for (a) wind speed error and (b) backscatter error for ASCAT rev 19221 (July 3, 2010). The upper and middle subplots show values of g and b, the numbers of pixels inside and outside the EMPSR region classified as oil. The lower subplots show $f(\nu)$, the objective function. Vertical axis scaling is arbitrary. The minimum of the function is indicated as a solid diamond.

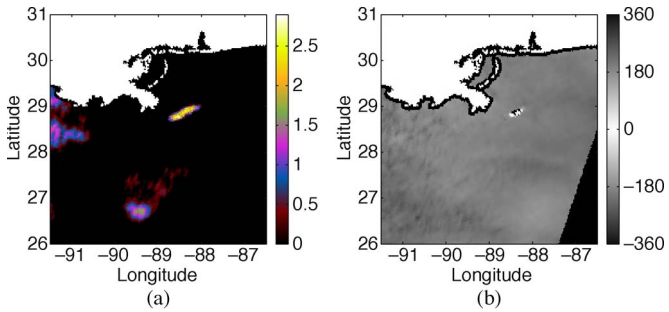

Fig. 2. Wind speed error and wind direction error for rev 18298 (April 29 2010). No EMPSR data are available to validate oil extent for this day. Wind speed errors are clipped to positive error only, i.e., pixels with ECMWF wind speeds less than ASCAT wind speeds are set to zero. Land and near-land ocean regions are masked off.

to obtain the backscatter error. Oil extent estimates are found after thresholding the errors, where error above the threshold is classified as oil. These are analyzed hereinafter. A case study is also presented comparing backscatter error with measured backscatter.

A. Wind Error

As described previously, the wind speed error and wind direction error are computed for all available ASCAT passes over the oil spill region. From one of the chosen case studies, the wind errors are shown in Fig. 2. Negative wind speed errors are discarded to reflect the expectation of positive error values caused by surface oil. The large values of $\epsilon_{|U_{10}|}$ near the center map the surface oil extent. Unfortunately, no EMPSR data are available on this particular day for validation.

The results in Fig. 2 suggest that the wind direction error is not as useful as wind speed error in surface oil mapping. In the best cases, wind direction error varies widely over a small region that is a subset of the oil region mapped by wind speed error. Fig. 2 shows a rare case where the wind direction error is well correlated with the oil spill. Wind direction error may be useful for determining the regions most affected by oil.

For comparison, the wind speed error is shown for two ASCAT passes in Fig. 3(a) and (c). The wind speed error for

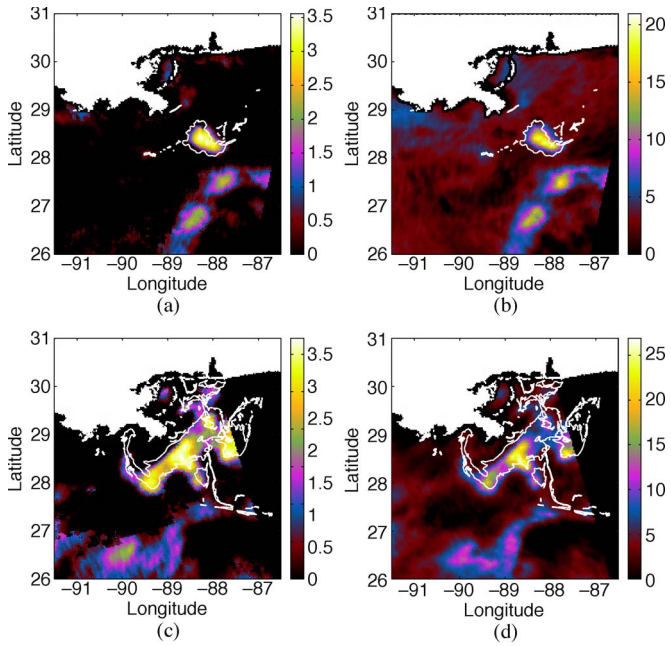

Fig. 3. Wind speed and backscatter errors for two ASCAT passes. The top row [subfigures (a) and (b)] is ASCAT rev 19363 (July 13, 2010), and the bottom row [subfigures (c) and (d)] is ASCAT rev 18745 (May 31, 2010). The left column [subfigures (a) and (c)] shows the wind speed error, and the right column [subfigures (b) and (d)] shows the backscatter error. EMPSR data are included in all subfigures as a white outline for validation. Negative errors are clipped to zero, as indicated in the text.

both passes strongly correlates with the main body of the oil spill. Smaller scale oil features are not detectable, however. Some false positives occur below the mapped oil. These are primarily due to the difference in inherent resolution in ASCAT data and ECMWF data. However, for the main body of surface oil, results from these and other passes show that wind speed error is a good match with the EMPSR data.

B. Backscatter Error

The backscatter error $\|\bar{\epsilon}\|_2$ is found for all available ASCAT passes over the oil spill. The backscatter error is shown for two ASCAT passes in Fig. 3(b) and (d). Negative backscatter error is discarded in these and other figures since only positive values are anticipated to indicate surface oil. The EMPSR data are shown by the white outlines. The results closely match the EMPSR data.

A comparison of the various metrics used to map the oil spill is shown in Fig. 4. The wind speed error [Fig. 4(a)] and backscatter error [Fig. 4(c)] map the bulk of the oil similarly. The differences between the two are typical of other passes and are discussed more hereinafter. The wind direction error is shown in Fig. 4(b). The direction error is largely uniform except for large errors near the oil rig location (not marked in the figure). Typically, these large direction errors are not found in other locations. It appears that the wind direction error only detects regions most affected by oil. For most ASCAT passes, both wind speed error and backscatter error validate well with EMPSR data.

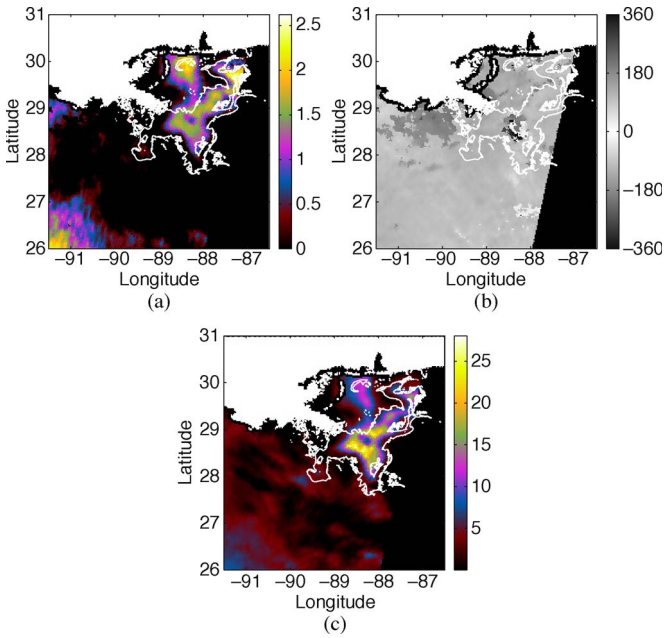

Fig. 4. Wind and backscatter errors for ASCAT rev 18880 (June 9, 2010). The wind speed error is in (a), the wind direction error in (b), and backscatter error in (c). In all subfigures, the EMPSR data are outlined in white for comparison. Negative values of backscatter error and wind speed error are discarded, as explained in the text.

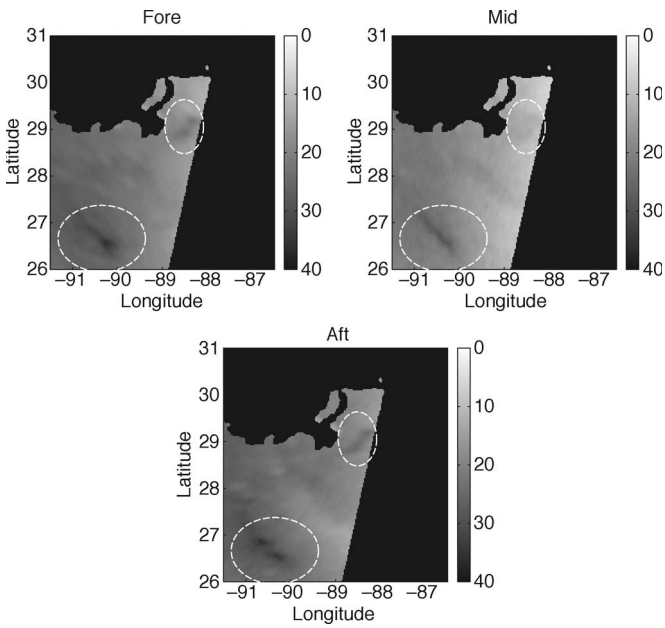

Fig. 5. ASCAT σ° (in decibels) fore, middle, and aft looks for rev 19221 (July 3, 2010). Fore and aft looks span incidence angles of 36°–55°, and the middle look spans a range of 27°–44°. The falloff of σ° with incidence angle accounts for the brightness variations across the swath. The locations of the two oil spill candidate regions are indicated with dashed ellipses.

C. Backscatter Versus Backscatter Error Case Study

As the previous results show, mapping the oil extent using wind speed error or backscatter error is generally effective. To illustrate the advantage of finding the backscatter error rather than using only the measured backscatter, we use the results of ASCAT rev 19221 (July 3, 2010) as a case study.

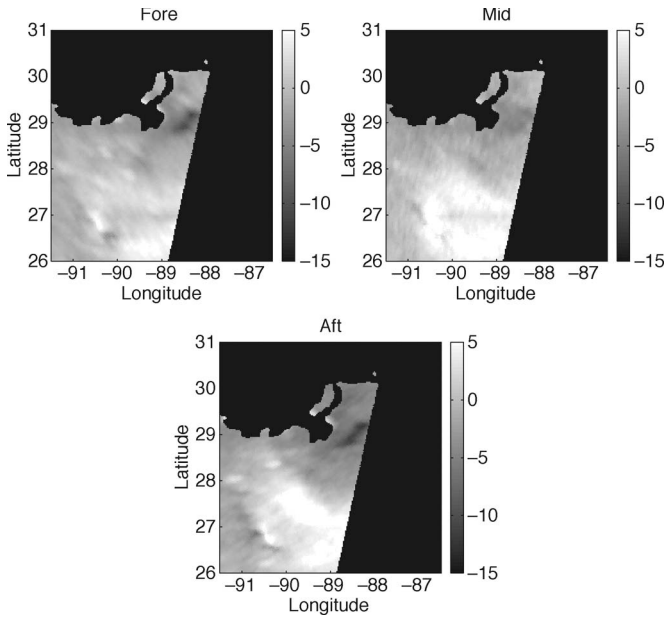

Fig. 6. Difference in decibels between measured and predicted σ° values for ASCAT rev 19221 (July 3, 2010). Compare with Fig. 5. The oil region is not as visible in the middle look due to the different incidence angles between the fore/aft and middle looks.

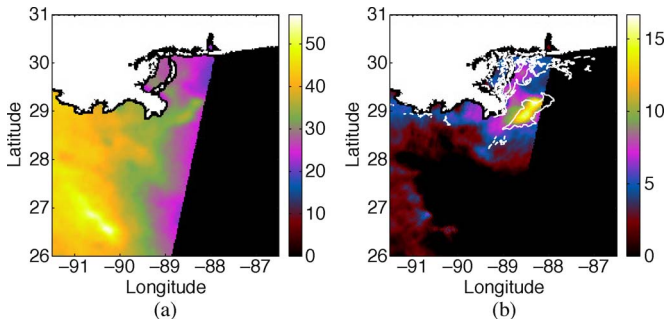

Fig. 7. ℓ_2 norm of the measured σ° in (a) and the ℓ_2 norm of the difference between measured and predicted σ° values in (b). Data from ASCAT rev 19221 (July 3, 2010) are used, along with interpolated ECMWF winds for (b). Land is masked out, and near-coastal regions are set to zero to remove biased wind estimates. The bright area in (b) indicates suppressed σ° measurements due to the presence of surface oil. The white outline is the EMPSR analysis for the surface oil extent.

Fig. 5 shows the high-resolution σ° field over each of the three looks for an ascending pass of ASCAT. In these images, two potential oil regions can be seen: one east of the Mississippi River Delta and one further south of the delta. The regions are noted with dashed ellipses. Similarly, Fig. 6 shows the difference between the measured and the predicted backscatter for each of the three looks. In Fig. 6, the region south of the delta with low wind speeds is accounted for, leaving only the oil region east of the delta visible.

Without using the predicted backscatter, combining the three looks in Fig. 5 using the ℓ_2 norm results in Fig. 7(a). The middle look (the center image in Fig. 5) spans a lower incidence angle range than the other two, leading to poor detection of the first oil candidate region. The ℓ_2 norm of the three looks has a greater value for the second candidate region than the first. The second region is a false positive due to low wind speeds in the area.

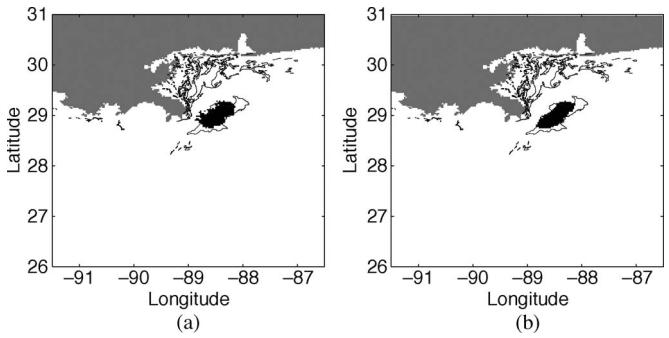

Fig. 8. Mapped oil extent using (a) wind speed error and (b) backscatter error for ASCAT rev 19221 (July 3, 2010). The gray region is land, and the black region is the error exceeding the chosen threshold. For comparison, the EMPSR region outline is overlaid in the figures as black lines.

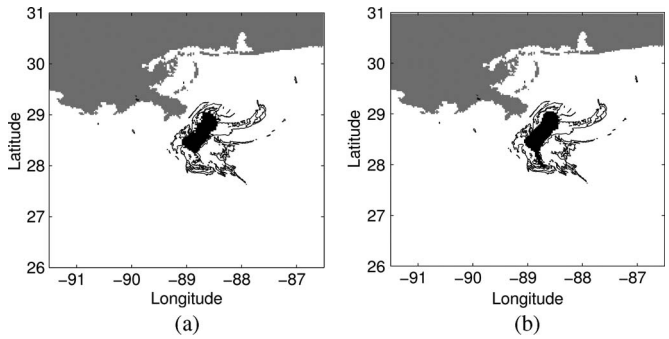

Fig. 9. Mapped oil extent using (a) wind speed error and (b) backscatter error for ASCAT rev 19434 (July 18, 2010). The gray region is land, and the black region is the error exceeding the chosen threshold. For comparison, the EMPSR region outline is overlaid in the figures as black lines.

Using (5) to merge the three looks in Fig. 6 to find the backscatter error results in Fig. 7(b). The white outline is the EMPSR product for the day. In this case, the results agree well with the largest EMPSR oil region, while the smaller regions near the coast are not as well detected.

D. Discussion

The EMPSR results corroborate the thresholded wind speed error and backscatter error during the middle of the spill (late April–mid-July) but are less effective near the beginning or end of the spill. It appears that, at these times, the presence of surface oil does not dampen σ° enough to be detectable by ASCAT. This could be due to the oil collection/burning efforts, weather conditions, or other factors.

Each pixel in the figures corresponds to an area of the ocean of about 5 km^2. It is unlikely that an area of that size is uniformly affected by oil, particularly on the boundary of the spill. Thus, due to the nonuniform beam filling, the true oil extent can only be approximated by ASCAT.

The wind direction error appears to only map an extent that is much smaller than that mapped by the wind speed or backscatter errors. Many ASCAT passes do not have any significant wind direction error, but for the passes that do, the errors often appear near the oil rig location, perhaps correlated with regions with thicker surface oil. We cannot validate this with EMPSR data, since no measurements of oil volume or thickness are reported in the EMPSR data set.

Wind speed error and backscatter error each correlate well with the EMPSR oil extent. The main body of surface oil is detectable by either of these methods, but smaller regions further from the center of the spill are usually less detectable. The biggest difference between wind speed error and backscatter error is the noise floor of the non-oil regions. The backscatter error images have a much higher noise floor than the wind speed error images. However, the wind speed error images have more false positives than the backscatter error images. When finding the optimum threshold value, these false positives tend to dominate the effects of the higher noise floor in the backscatter error images.

The optimum threshold is selected for each pass. Using this threshold, a comparison of detected oil with EMPSR data is shown in Figs. 8 and 9 for two different ASCAT passes. The chosen threshold maximizes true positives (flagged pixels within the EMPSR boundary) and minimizes false positives (flagged pixels outside the EMPSR boundary) with relative weighting controlled by α in (6). These results are typical of other passes. Generally, thresholded backscatter error has fewer false alarms than thresholded wind speed error. A subset of the processed thresholded backscatter error images is shown in Fig. 10. While the oil spill is mapped well by many of the passes, other passes contain wind-speed-induced oil look-alikes. The low wind speeds of these regions (about 3 m/s or less) make oil detection difficult with the methods presented here.

V. Conclusion

Although originally designed for only low-resolution ocean wind measurements, ASCAT can be used to map the surface extent of large bodies of oil on the ocean surface. The detection of ocean surface oil by active microwave instruments is based on a contrast of σ° over oil-affected areas and oil-free areas. Moderate wind speeds sufficiently roughen the ocean surface to provide this contrast. A comparison of σ° values while accounting for the wind over the oil improves the detection.

Accounting for the wind may be done directly in the wind domain, or it may be done in the backscatter domain by finding the predicted backscatter based on the reference winds and the GMF. Both approaches have been explored in this paper. The methods presented in this paper account for the near-surface wind by using the ASCAT GMF in conjunction with NWP winds to compute several oil-mapping metrics: the wind speed error $\epsilon_{|U_{10}|}$, the wind direction error $\epsilon_{\angle U_{10}}$, and the norm of the backscatter errors $\|\bar{\epsilon}\|_2$.

The wind speed error and backscatter error both match EMPSR products to a higher degree than wind direction error. While the amount of true positives is typically similar between the two, wind speed error generally has more false positives than backscatter error, and backscatter error exhibits a higher noise floor. Both metrics are useful for mapping surface oil extent, but using a threshold to categorize the pixels in a binary

Fig. 10. Selected time series of mapped oil. Each image is the thresholded backscatter error for the date indicated in the upper left corner. The ASCAT pass may not completely cover the region on a given day, leading to a diagonal crop in some of the images.

manner generally works better using thresholded backscatter error. The wind direction error $\epsilon_{\angle U_{10}}$ may provide some indication of where the surface oil is most dense.

Small oil regions in EMPSR data are not usually resolvable in wind speed and backscatter errors. However, the main body of surface oil is mapped effectively. The backscatter error and wind speed error results presented show a good match with conventional oil detection techniques making use of multiple sensors as reported in the EMPSR product. False positives or oil "look-alikes" still arise owing to the limitations of working with a single instrument, but the occurrence of wind-related false alarms is diminished. Results validate well with EMPSR results except for the very beginning and end of the spill.

REFERENCES

[1] T. J. Crone and M. Tolstoy, "Magnitude of the 2010 Gulf of Mexico oil leak," *Science*, vol. 330, no. 6004, p. 634, Sep. 2010.

[2] C. Brekke and A. Solberg, "Oil spill detection by satellite remote sensing," *Remote Sens. Environ.*, vol. 95, no. 1, pp. 1–13, Mar. 2005.

[3] M. Migliaccio, A. Gambardella, and M. Tranfaglia, "SAR polarimetry to observe oil spills," *IEEE Trans. Geosci. Remote Sens.*, vol. 45, no. 2, pp. 506–511, Feb. 2007.

[4] M. Migliaccio, F. Nunziata, A. Montuori, X. Li, and W. G. Pichel, "A multifrequency polarimetric SAR processing chain to observe oil fields in the Gulf of Mexico," *IEEE Trans. Geosci. Remote Sens.*, vol. 49, no. 12, pt. 1, pp. 4729–4737, Dec. 2011.

[5] A. H. S. Solberg, C. Brekke, and P. O. Husoy, "Oil spill detection in RADARSAT and Envisat SAR images," *IEEE Trans. Geosci. Remote Sens.*, vol. 45, no. 3, pp. 746–755, Mar. 2007.

[6] J. Figa-Saldaña, J. J. W. Wilson, E. Attema, R. Gelsthorpe, M. R. Drinkwater, and A. Stoffelen, "The Advanced Scatterometer (ASCAT) on the Meteorological Operational (MetOp) platform: A follow on for European wind scatterometers," *Can. J. Remote Sens.*, vol. 28, no. 3, pp. 404–412, 2002.

[7] F. Naderi, M. Freilich, and D. Long, "Spaceborne radar measurement of wind velocity over the ocean—An overview of the NSCAT scatterometer system," *Proc. IEEE*, vol. 79, no. 6, pp. 850–866, Jun. 1991.

[8] H. Hersbach, "CMOD5.N: A C-band geophysical model function for equivalent neutral wind," ECMWF, Reading, U.K., 2008, Tech. Rep..

[9] S. Shaffer, R. Dunbar, S. Hsiao, and D. Long, "A median-filter-based ambiguity removal algorithm for NSCAT," *IEEE Trans. Geosci. Remote Sens.*, vol. 29, no. 1, pp. 167–174, Jan. 1991.

[10] A. Stoffelen, S. de Haan, Y. Quilfen, and H. Schyberg, "ERS scatterometer ambiguity removal scheme comparison," Roy. Netherlands Meteorol. Inst., De Bilt, The Netherlands, 2000.

[11] R. D. Lindsley and D. G. Long, "Adapting the SIR algorithm to ASCAT," in *Proc. IEEE IGARSS*, 2010, pp. 3402–3405.

[12] D. G. Long, P. Hardin, and P. Whiting, "Resolution enhancement of spaceborne scatterometer data," *IEEE Trans. Geosci. Remote Sens.*, vol. 31, no. 3, pp. 700–715, May 1993.

[13] D. S. Early and D. G. Long, "Image reconstruction and enhanced resolution imaging from irregular samples," *IEEE Trans. Geosci. Remote Sens.*, vol. 39, no. 2, pp. 291–302, Feb. 2001.

[14] B. A. Williams and D. G. Long, "Reconstruction from aperture-filtered samples with application to scatterometer image reconstruction," *IEEE Trans. Geosci. Remote Sens.*, vol. 49, no. 5, pp. 1663–1676, May 2011.

[15] M. P. Owen and D. G. Long, "Simultaneous wind and rain estimation for QuikSCAT at ultra-high resolution," *IEEE Trans. Geosci. Remote Sens.*, vol. 49, no. 6, pp. 1865–1878, Jun. 2011.

[16] F. Ulaby, R. Moore, and A. Fung, *Microwave Remote Sensing: Active and Passive*, vol. 2, D. Simonett, Ed. Norwood, MA: Artech House, 1986.

[17] P. Clemente-Colón and X. Yan, "Low-backscatter ocean features in synthetic aperture radar imagery," *Johns Hopkins APL Tech. Dig.*, vol. 21, no. 1, pp. 116–121, 2000.

[18] W. Alpers, "Remote sensing of oil spills," in *Proc. Maritime Disaster Manage. Symp.*, 2002, pp. 19–23.

[19] B. Zhang, W. Perrie, X. Li, and W. G. Pichel, "Mapping sea surface oil slicks using RADARSAT-2 quad-polarization SAR image," *Geophys. Res. Lett.*, vol. 38, p. L10 602, 2011.

[20] C. Nie and D. G. Long, "A C-band scatterometer simultaneous wind/rain retrieval method," *IEEE Trans. Geosci. Remote Sens.*, vol. 46, no. 11, pp. 3618–3631, Nov. 2008.

[21] M. Donelan and W. Pierson, Jr., "Radar scattering and equilibrium ranges in wind-generated waves with application to scatterometry," *J. Geophys. Res.*, vol. 92, no. C5, pp. 4971–5029, 1987.

[22] F. Girard-Ardhuin, G. Mercier, F. Collard, and R. Garello, "Operational oil-slick characterization by SAR imagery and synergistic data," *IEEE J. Ocean. Eng.*, vol. 30, no. 3, pp. 487–495, Jul. 2005.

[23] NOAA/NESDIS, Satellite Derived Surface Oil Analysis Products—Deepwater Horizon. [Online]. Available: http://www.ssd.noaa.gov/PS/MPS/deepwater.html

Richard D. Lindsley (S'08) received the B.S. degree in electrical engineering from Brigham Young University (BYU), Provo, UT, in 2009, where he is currently working toward the Ph.D. degree.

Since 2008, he has been with the Microwave Earth Remote Sensing Laboratory, BYU. His research interests include microwave remote sensing and signal processing.

David G. Long (S'80–SM'98–F'08) received the Ph.D. degree in electrical engineering from the University of Southern California, Los Angeles, in 1989.

From 1983 to 1990, he was with the Jet Propulsion Laboratory (JPL), National Aeronautics and Space Administration (NASA), where he developed advanced radar remote sensing systems. While at JPL, he was the Project Engineer on the NASA Scatterometer project which flew from 1996 to 1997. He also managed the SCANSCAT project, the precursor to SeaWinds which was launched in 1999 on QuikSCAT and 2002 on ADEOS-II. He is currently a Professor with the Electrical and Computer Engineering Department, Brigham Young University (BYU), Provo, UT, where he teaches upper division and graduate courses in communications, microwave remote sensing, radar, and signal processing and is the Director of the BYU Center for Remote Sensing. He is the Principal Investigator on several NASA-sponsored research projects in remote sensing. He has over 400 publications in various areas, including signal processing, radar scatterometry, and synthetic aperture radar. His research interests include microwave remote sensing, radar theory, space-based sensing, estimation theory, signal processing, and mesoscale atmospheric dynamics.

Dr. Long is an Associate Editor for IEEE GEOSCIENCE AND REMOTE SENSING LETTERS. He was a recipient of the NASA Certificate of Recognition several times.